Modelling of dripwater hydrology and hydrogeochemistry in a weakly karstified aquifer (Bath, UK): Implications for climate change studies

Ian J. Fairchild[a,*], George W. Tuckwell[b], Andy Baker[a], Anna F. Tooth[c]

[a]School of Geography, Earth and Environmental Sciences, University of Birmingham, Edgbaston, Birmingham B15 2TT, UK
[b]STATS Geophysical, Porterswood House, Porters Wood, St Albans, Herts AL3 6PQ, UK
[c]Groundwater Protection, Environment Agency, Worthing, W Sussex BN11 1LD, UK

Abstract

A better knowledge of dripwater hydrology in karst systems is needed to understand the palaeoclimate implications of temporal variations in Mg/Ca and Sr/Ca of calcareous cave deposits. Quantitative modelling of drip hydrology and hydrochemistry was undertaken at a disused limestone mine (Brown's Folly Mine) in SW England overlain by 15 m of poorly karstified Jurassic limestones, with sub-vertical fracturing enhanced by proximity to an escarpment. Discharge was monitored at 15 sites intermittently from the beginning of 1996, and every 10–20 days from later 1996 to early 1998. Samples for hydrochemical parameters (pH, alkalinity, cations, anions, fluorescence) were taken corresponding to a sub-set of these data and supplemented by bedrock and soil sampling, limited continuously logged discharge, and soil water observations. Three sites, covering the range of discharge (approximately 1 μL s^{-1} to 1 ml s^{-1} maximum discharge) and hydrochemical behaviours, were studied in more detail. A quantitative flow model was constructed, based on two parallel unit hydrographs: responsive and relatively unresponsive to discharge events, respectively. The linear response and conservative mixing assumptions of the model were tested with hydrogeochemical data.

Dripwaters at many of sites are characterized by evidence of prior calcite precipitation in the flowpath above the mine, which in the higher discharging sites diminishes at high flow. Also at low flow rates, dripwaters may access seepage reservoirs enriched in Mg and/or Sr, dependent on the site. The discharge at all three sites can be approximated by the flow model, but in each case, hydrochemical data show violations of the model assumptions. All sites show evidence of non-conservative mixing, and there are temporal discontinuities in behaviour, which may be stimulated by airlocks generated at low flow. Enhanced Mg/Ca and Sr/Ca often do relate to low-flow conditions, but the relationships between climate and hydrogeochemical response are non-linear.
© 2005 Elsevier B.V. All rights reserved.

Keywords: Hydrogeochemistry; Karstic aquifer; Modelling, Stalagmite palaeoclimate

1. Introduction

Low discharges of dripwaters into karst caves can be of great importance when they deposit stalactites or

---

* Corresponding author.
  E-mail address: i.j.fairchild@bham.ac.uk (I.J. Fairchild).

stalagmites (speleothems). Such accretions preserve records interpretable in terms of the past hydrologic and climatic conditions. Trace element records from the stalagmites can be linked to the changing geochemistry and the saturation state of dripwaters on time periods varying from sub-seasonal to multi-year (Fairchild et al., 2001; Huang et al., 2001; McMillan et al., 2005). Reliable interpretation of the past records is greatly enhanced by a good under-standing of the modern hydrologic processes in the cave. The overall aim of this study is to provide a quantitative illustration of the extent to which the geochemistry of dripwaters shows a direct and simple response to variations in the rate of infiltrating water, as has been found for example for karstic springs (Long and Derickson, 1999). In particular, if waters become enriched in trace elements at low flow (Baker et al., 2000) then they would precipitate a stalagmite layer whose chemistry reflects these low-flow con-ditions and hence can be diagnostic of relatively dry weather or climatic conditions above ground.

Cave dripwaters are unsaturated zone phenomena and the properties of each drip are individual and related to complex flow routes with limited lateral dispersion (Bottrell and Atkinson, 1992). Discharge studies indicate a wide variety of responses to infiltrating water, with the variation in drip rate increasing with mean discharge (Smart and Friederich, 1986), indicative of an increased proportion of flow through relatively faster routes. The flow rate typically varies with seasonal changes in water infiltrated into the aquifer and may respond to short-term pressure changes (Genty and Deflandre, 1998). Studies using natural organic tracers show that a new soil-derived component of the water flow takes from days to months to reach the cave site (Baker et al., 1999, 2000). Hydrogeochemical studies indicate both the derivation of water from different storage sources, and the variable modification of water chemistry by calcite precipitation en route to the cave (Baker et al., 2000; Fairchild et al., 2000; Tooth and Fairchild, 2003).

Our first objective in this paper is to present a new set of hydrological and hydrogeochemical dripwater data from an established study site (Baker et al., 1999; Baker and Genty, 1999) which constrain some aspects of an appropriate quantitative model structure, including the necessity for mixing processes and prior calcite precipitation. Secondly, we have

constructed and tested a linear systems model against the data. This has led to a more detailed understanding of non-linearities in the system.

2. Study site

The site is a 19th-century stone mine which provides unusually ready access to the interior of a near-surface weakly karstified aquifer. Brown's Folly Mine (at 51° 23'W, 2° 22'N; National Grid reference ST795660) was described by Baker et al. (1999); only essential details are repeated here, together with additional information on the aquifer. The geological setting is simple: a NNW–SSE flat-topped escarpment is underlain by a horizontally stratified succession (Green and Donovan, 1969) of Middle Jurassic oolitic and shelly limestones (Fig. 1) in which vertical fractures ('gull rifts', Self, 1995) tend to develop parallel to the scarp topography. This major set of fractures provides the major fissure flow, although there is a 25 cm-thick clay layer within the aquifer that may inhibit flow. Slower flow should occur along more minor fissures and by seepage from water stored within the porous limestone matrix. Thin section analysis confirms that limestone lithologies are mainly oolitic and skeletal (fossiliferous) limestones with minor sand and clay. Shelly fragments and some ooids that were originally composed of aragonite are leached and cemented by calcite. Some isolated dolomite crystals were found in one sample. Porosity varies from zero to 40% and is quite heterogeneous between beds and within some beds.

A thin brown forest soil is developed. Typically 25 cm thick, it consists of a litter horizon on a clay soil with peds and rootlets and root macropores. The lower half of the profile contains blocks derived from the underlying limestone. Native deciduous woodland has established over the site since the abandonment of the mine operation in 1904. In the mine itself, abandoned rooms into which dripwater seeps contain soda straw stalactites and small stalagmites. Apart from some poorly ventilated rooms, the bulk of the mine is at atmospheric PCO_2 which facilitates degassing of the dripwater and precipitation of $CaCO_3$.

The area experiences a maritime temperate climate. Mean annual temperature at Bristol (22 km to the west) is 10.0 °C with a winter monthly
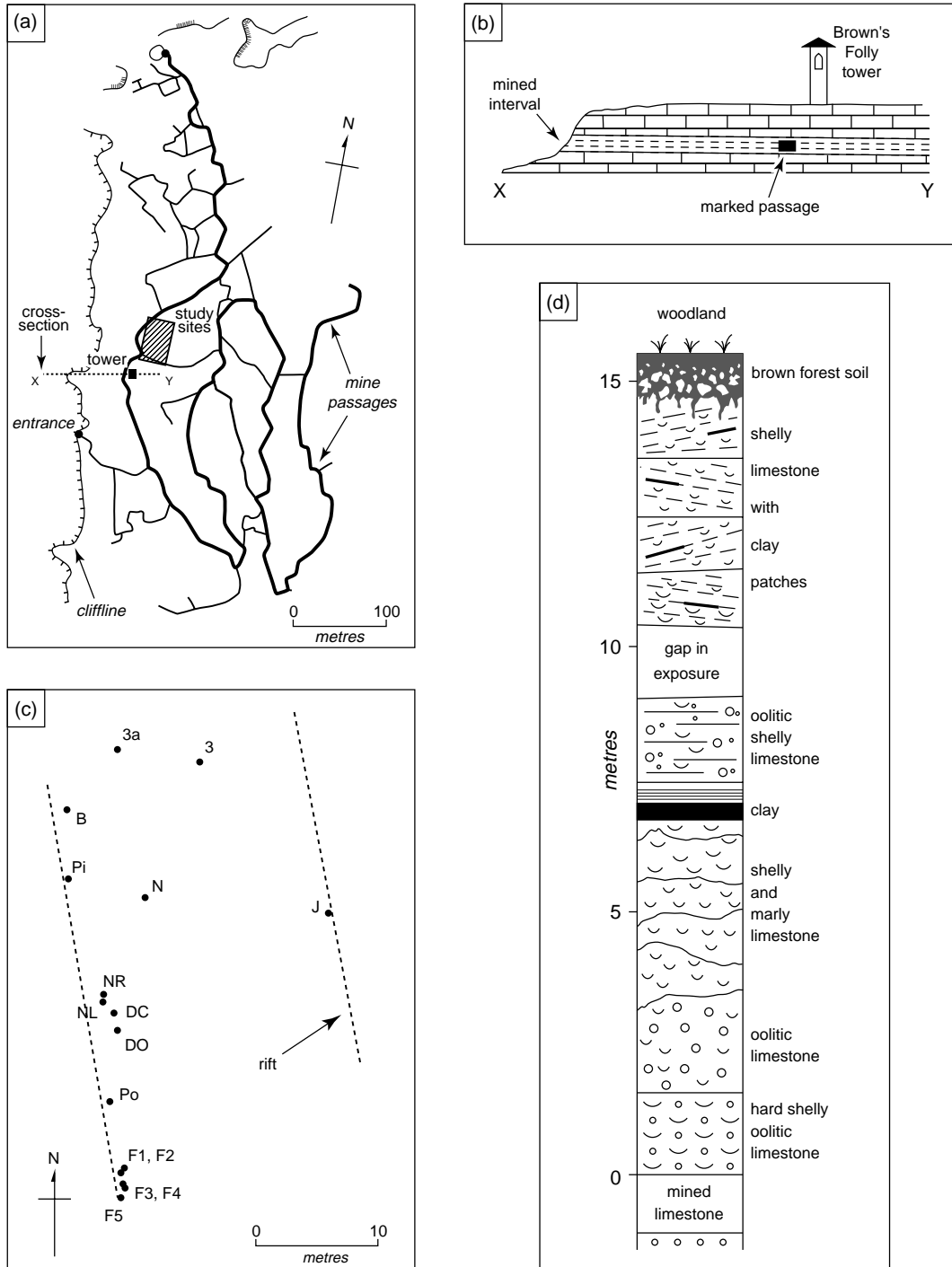
Fig. 1. Location of study site and geological properties of host aquifer. (a) locations of study sites in relation to mine workings and escarpment. (b) sketch cross-section along line X-Y on map (a) (no vertical exaggeration). (c) section of the approximately horizontal strata of the aquifer overlying the mine workings. (d) detailed location of study sites and schematic position of tensional fracture zones ("rifts", Baker et al., 1999).

minimum of 3.9° with snow lying rarely, and summer monthly maximum of 16.5°. Mean annual precipitation is 842 mm.

The cave was monitored over the period of 1996–1997: a relatively dry year, with 595 mm precipitation, was recorded 3 km away at Bathford in 1996, followed by a more average year (818 mm) in 1997. In both years substantial periods of infiltration were calculated to occur in the winter (Baker et al., 1999) in response to frontal rains, but there was also evidence from increased drip rates that short-term summer rainfall also caused infiltration. Data on the fluorescence of slow-discharge dripwaters demonstrated increases in soil-derived components typically 10–20 days after periods of heavy infiltration (Baker et al., 1999).

3. Chemical and hydrological methods

Following some initial visits in 1996, 16 dripwater sites were monitored at intervals of 10–20 days from November 1996 to April 1998. Their discharge was measured and in most cases dripwaters were also sampled (in full glass bottles). Discharge was measured by manual observation of the rate of dripping, supplemented to a limited extent by automated drip counting. A sub-set of samples was measured for pH in the field with a Sentron probe with an error of 0.1 units, whilst in the laboratory waters

were filtered and analyzed for conductivity ($\pm 1\%$) and alkalinity ($\pm 3\%$). Ion analysis, with analytical errors of typically $\pm 5\%$, was carried out at the University of Exeter by atomic absorption spectrometry for cations on acidified samples (Ca, Mg, Na, K and Sr) and on around half the samples by ion chromatography for chloride and sulphate. Fluorescence analysis of dissolved organic species was carried out on another aliquot (Baker et al., 1999). Two soil water samples were also extracted from a soil lysimeter installed in June 1997. The cation leachates from 15 sub-samples of 10 rock samples from different levels, together with six soil samples, were characterized by dissolution of aliquots of powdered samples in dilute hydrochloric acid for analysis of Ca, Mg, Sr and insoluble residue.

Potential evapotranspiration was estimated by Baker et al. (1999) using the UK Meteorological Office's MORECS system and in this study was calculated from monthly temperature data using the Thornthwaite method (Shaw, 1994), which is found to give similar results. The karstic modelling methodology is explained later.

4. Hydrology and hydrogeochemistry of the dripwaters

Fig. 2 summarizes the mean discharge of drip sites in relation to the variation in discharge plotted on
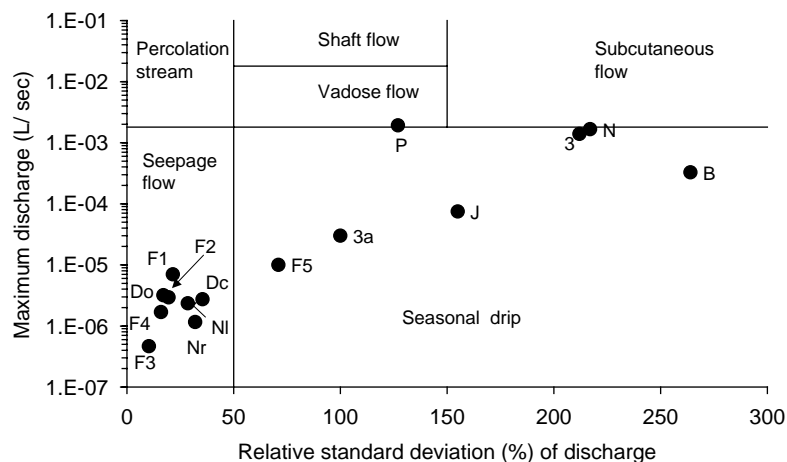

Fig. 2. Hydrological behaviour of drip sites (Fig. 1d) expressed in terms of maximum discharge versus variability in discharge (see also Table 1 for other properties). Measured drip rates (as plotted in other figures) are converted to volume units assuming a drip volume of 0.15 ml.

Table 1
Summary hydrology, cation hydrogeochemistry and inferred processes for dripwater sites at Browns Folly Mine

Site	Relative standard deviation of discharge (%)	Maximum discharge (μL/s)	Mean discharge (μL/s)	Mean discharge (drips/ks)	Minimum Mg/Ca (molar)	Minimum 1000 Sr/Ca (molar)	Mg-rich source at low flow	Sr-rich at low flow	Prior calcite precipitation	Dilution at high flow
B	**264**	**330**	**34**	**227**	**0.074**	**1.9**	**yes**	**no**	**yes**	**no**
N	217	1670	231	1540	0.074	no data	yes	no data	yes	no
3	212	1390	174	1160	0.075	no data	yes	no data	yes	rare
J	155	75	12	82.2	0.066	1.9	no	varies	yes	no
P	127	1920	386	2570	0.065	no data	yes	no data	yes	rare
3a	100	30	5.1	34	0.077	no data	yes	no data	?no	no
F5	**71**	**10**	**3.6**	**24**	**0.067**	**2.5**	**?**	**no**	**yes**	**no**
DC	35	2.7	1.0	6.8	0.070	1.4	yes	yes	yes	no
NR	32	1.2	0.7	4.8	0.098	1.6	no	yes	no	no
NL	29	2.4	1.8	11.9	0.076	2.5	no	no	no	no
F1	22	7.0	5.4	36.2	0.071	0.5	no	yes	no	no
F2	20	2.9	2.3	15.2	0.082	2.1	no	no	no	no
DO	17	3.2	2.5	16.9	0.072	1.6	no	no	no	no
F4	16	1.7	1.3	8.5	0.074	1.6	no	yes	no	no
F3	**10**	**0.5**	**0.4**	**2.6**	**0.078**	**0.8**	**no**	**yes**	**yes**	**no**

The three sites chosen for detailed analysis are shown in bold. The significance of the minimum Mg/Ca and Sr/Ca values and prior calcite precipitation is explained in the text. Two sites show (rarely) some dilution effect at the highest discharges and some low discharge sites display apparent dilution effects which do not clearly relate to infiltration events.

the definition grid of Smart and Friederich (1986) as modified by Baker et al. (1997). As expected, the faster drips are also flashier, presumably in response to fissure flow. Table 1 summarizes some hydrogeochemical attributes of the drips that are relevant for modelling. Most drips respond rationally, i.e. they show variation in properties related to periods of recharge (Baker et al., 1999). The last four columns in Table 1 refer to particular types of rational hydrochemical response shown by particular drips. Nevertheless drips that are very close together (Fig. 1(c)) can show quite different hydrogeochemical properties, indicating the complexity of the aquifer plumbing. Three drips have been selected for more detailed analysis: drips B, F5 and F3 which cover the whole range of hydrological behaviour (Fig. 2). Between them they also illustrate most of the interesting hydrogeochemical behaviours shown in Table 1.

Some of the attributes of the drips show relationships with discharge, but we found no pronounced hysteresis effects (cf. Chanat et al., 2002). Calcium covaries positively with discharge (Fig. 3(a)) at site B, but only weakly at F5 (F3 shows

no co-variation). On the other hand, Mg varies inversely with discharge at site B (Fig. 3(b)); this is a property of many of the faster dripping sites (Table 1). The relationship at F5 is too weak to be definitive (Fig. 3(b)), although the lowest Mg values all occur at high flow. Sr tends to be higher at low discharge at site F3 and some of the other slow-dripping sites (Table 1). The other cations, and chloride and sulphate do not show any relationships with discharge.

Soil water samples were only recoverable immediately after heavy rain and Ca values did not exceed 2.1 mmol/L, implying undersaturation for $CaCO_3$ since higher values (up to 3 mmol/L) were obtained from some dripwaters indicating soil-derived high PCO_2 values of $10^{-1.3}$ or more (Fig. 4). Nevertheless, kinetic calculations (after Chou et al., 1989) indicate that saturation must occur within a couple of hours of percolation within the underlying calcareous soil base or epikarst. This is consistent with observations of cave dripwaters, which were consistently supersaturated for calcite, but less so at high discharge at site B. Here, the calculated calcite saturation index (the log ratio of ionic activity product to solubility
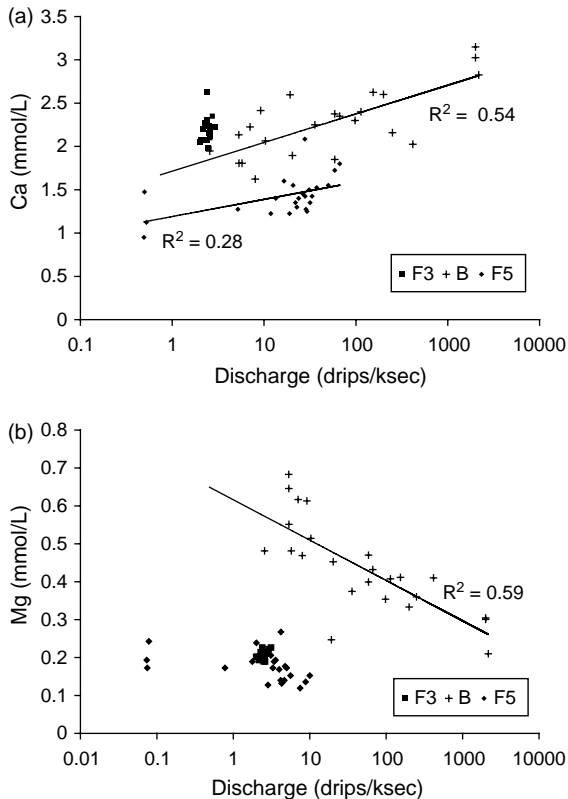
Fig. 3. Relationship of Ca and Mg concentrations with discharge. (a) Site B shows a good positive covariation of Ca with discharge, F5, a weak covariation and site F3 no covariation. (b) A strong negative relationship of Mg with discharge is shown by site B, a weak negative relationship is shown by F5 and site F3 shows no significant variation.

product) varied from around 0.1 at peak flow, with a PCO_2 of $10^{-2.0}$, to more typical values at lower flows of 0.5–0.8 at PCO_2 of around $10^{-3.0}$.

In addition to supersaturation within the mine chamber (both stalactites and stalagmites occur), it can be inferred that precipitation of $CaCO_3$ in the aquifer above the mine can occur, where the low PCO_2 mine air penetrates and allows CO_2 degassing to occur, which leads to strong supersaturation for calcite (calcite-coated fractures on the cave ceiling occur). Calcite precipitation is associated with a partition coefficient (K)

$$(Tr/Ca)_{CaCO_3} = K \times (Tr/Ca)_{solution}$$

where Tr stands for a trace element such as Mg or Sr. Values of K are $\ll 1$ (Morse and Bender, 1990;

Huang and Fairchild, 2001); hence, little of the trace element is removed from the water, so that the residual solution ratios of Mg/Ca and Sr/Ca rise. Fig. 4 illustrates guidelines to show the evolution of water composition in relation to this process (Fairchild et al., 2000). Mg/Ca for site F3 and Sr/Ca for sites B and F5 conform to the prior calcite precipitation behaviour. However, Mg/Ca for sites B and F5 show a more extreme enrichment in the trace elements at low Ca concentrations (corresponding to low flow conditions at B), implying the tapping of a reservoir relatively high in Mg/Ca at low flow. A similar behaviour is shown by Sr/Ca at site F3 at low flow (high Sr/Ca points on Fig. 4(b)). These relationships provide constraints on modelling these drips.

The minimum values of Mg/Ca and Sr/Ca found at a site thus would correspond to the compositions of water affected least by calcite precipitation or by minimal mixing with a source enriched in trace elements. In the case of Sr/Ca, the minimum values found are similar to the mean values of the bedrocks (0.0016). The higher values found at low flow at sites like F3 imply an additional source of Sr. This is probably from clay layers within which the original aragonitic $CaCO_3$ of certain molluscan fossils can be preserved, since aragonite is greatly enriched in Sr compared with calcite. A similar case is represented by the Grotte de Villars in France (Baker et al., 2000). In the case of Mg, the mean bedrock Mg/Ca (0.016, median 0.007) is much lower than the dripwaters. However, since there is typically 0.5 mmol/L of chloride in the waters, an additional marine aerosol source for Mg is indicated of around 0.06 mmol/L. This is sufficient to explain the difference between the bedrock values and the minimum Mg values at the drip sites. The source of the additional Mg at low flow in some drips is probably dolomite as no other Mg-rich phases were identified and the highest bedrock Mg/Ca value of 0.12 probably reflects the occurrence of dolomite. Dolomite dissolution would be enhanced, where the water residence time is longer, because of its slow dissolution kinetics (Fairchild et al., 2000). No consistent relationship was found between stratigraphic position and Mg or Sr content of bedrocks, so that no individual horizons can be identified as sources of seepage water.
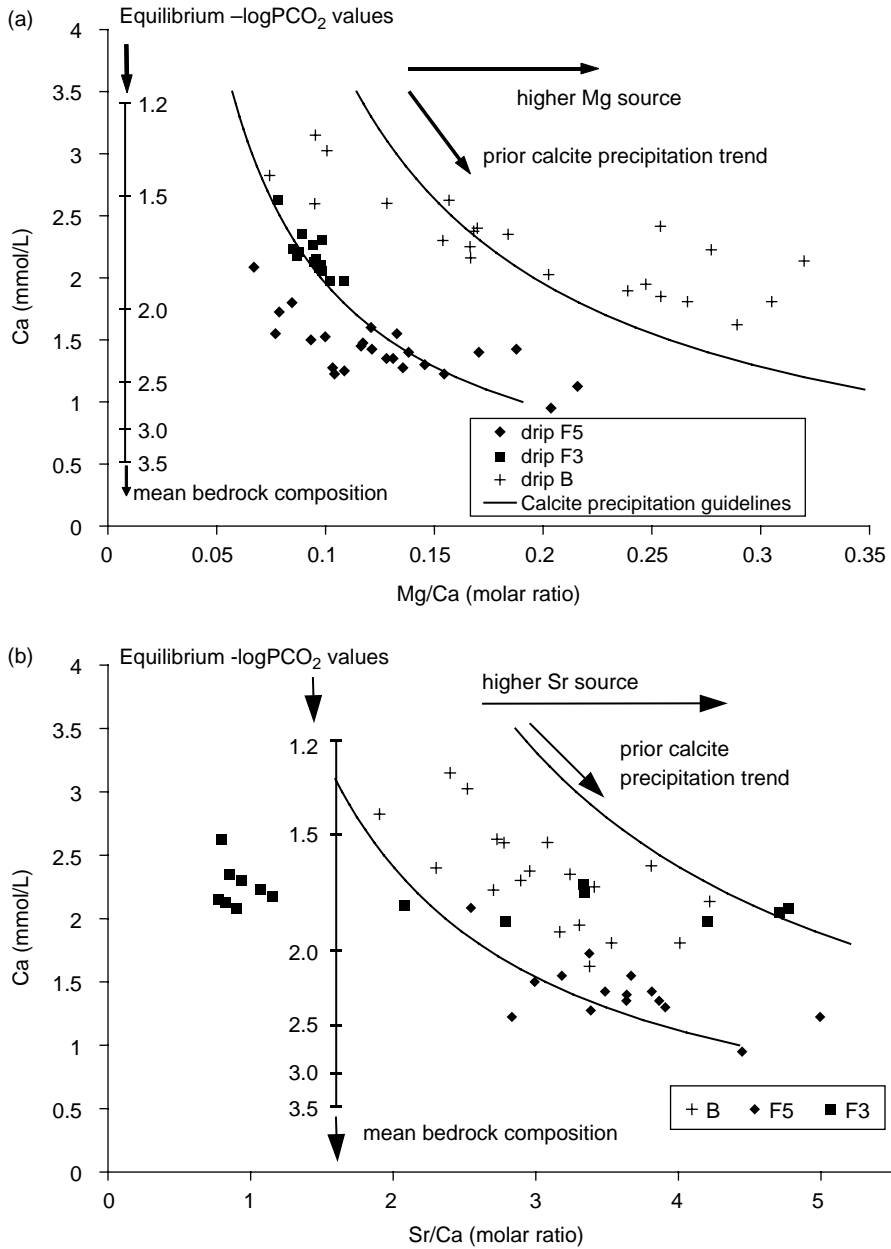
Fig. 4. Hydrochemical variations of dripwaters shown as plots of Ca versus Mg/Ca (a) and Sr/Ca (b). The Ca concentration of solutions in equilibrium with $CaCO_3$ at various values of PCO_2 is shown. The maximum value of Ca approaches that expected from the PCO_2 values of soil waters. The Mg/Ca of dripwaters is always much greater than of bedrock because of additional Mg in atmospheric precipitation, but the lower values of Sr/Ca of dripwaters are similar to mean bedrock compositions. Higher values of Mg/Ca and Sr/Ca arise from either precipitation of $CaCO_3$ along the flowpath (expected trend is shown by the calcite precipitation guidelines) or, where trends are more extreme than indicated by the guidelines, by tapping of a source rich in either Mg or Sr at low flow (see text). Summary of behaviour from all sites is given in Table 1.

5. Model philosophy and description

Tooth and Fairchild (2003) have recently constructed a conceptual model to account for hydrological and hydrogeochemical variations in dripwaters, based on examples from a natural cave system in Ireland. The model considers 'plumbing elements' (after Smart and Friederich, 1986) of seepage and fracture-fed flow, in addition to prior calcite precipitation upflow from the measured drip. The approach here is to envisage the simplest possible plumbing model that might explain the behaviour of the drips and to test whether such a simple model can explain the hydrological and hydrogeochemical variability encountered. The description of the hydrology and hydrogeochemistry in Section 4, with compositions of dripwaters being dependent on discharge, is consistent with the basic concepts of this model expressed as a combination of mixing and prior calcite precipitation.

Below, we develop this idea quantitatively as a linear systems model. Our modelling draws on previous approaches developed in different hydrological sub-fields, but the application to dripwater is novel. Karstic aquifers in general are triple-porosity aquifers (Smart, 1999), but we are not here concerned with major conduits as they are only locally represented by sinking streams in the study aquifer (Smart, 1977). The lower-flow parts of any fractured aquifer can in principle be simulated as a continuum with Darcian flow, or as matrix with a network of discontinuities represented as fractures or as conduits (Selroos et al., 2002). Each of these approaches has proved appropriate for karstic modelling (e.g. Vaute et al., 1997; Annabe and Sudicky, 1999; Maloszewski et al., 2002). We are concerned to separate relatively faster and slower flow components, but without distinction of their geometric form, since they are modelled as a simple parallel series of unit hydrograph responses to infiltrating rainwater. Although this is a linear systems approach, it is closer to the Nash cascade approach (Yue and Hashino, 2000; Beven, 2001), than the development of a single transfer function by Fourier methods as used by Long and Derickson (1999) for example. However, in its use of certain non-linear responses such as accounting for evapotranspiration, and allowing for reservoir overflow, it relates to the ESMA (explicit soil

moisture accounting) family of models which are widely used in river catchment hydrology (Beven, 2001). A feature of our approach is to find optimal solutions to the model to fit the observed flows and to test these predictions against an assumption of conservative mixing, using the dripwater hydrochemistry, since conservative mixing is the default assumption in surface water hydrograph separation by geochemical techniques (Buttell, 1994). In the literature, oxygen isotopes have normally been used as the mixing tracer (e.g. Perrin et al., 2003; Long and Putnam, 2004), which is conservative by definition. We have used elemental chemistry since it relates to our ultimate aim of understanding stalagmite geochemistry. We make the key assumption that trace elements will be conserved during short-term mixing, and re-examine this assumption in the discussion.

In geochemical terms, the vadose system should be modelled in terms of a two-layer geometry (Tooth and Fairchild, 2003). In the upper layer, carbonate dissolution takes place in high-PCO_2 conditions, whereas lower in the karst system, opportunities for degassing into an air space of lower PCO_2 arise and it is this that stimulates speleothem formation.

In our implementation, the upper layer (layer 1) combines soil and upper epikarst (for simplicity one can think of it as a high PCO_2 system governed by CO_2 production in the soil). This corresponds to a dual-porosity system that is simplified in our modelling (Fig. 5) to two elements each with different characteristic unit hydrographs. The lower layer (2) is one in which our model is concerned only with two processes: firstly, mixing from the upper system waters and secondly, the effects of low PCO_2 resulting from ventilation of the underlying cave system, particularly at low flow, and resulting in calcite precipitation.

Two principal types of hydrograph are used to represent macropore flow, and matrix flow. The macropore hydrograph refers to an enhanced flow through soil macropores and karstic fissures, which are known at the study site, and which elsewhere are known to be actively involved in aquifer recharge during rainfall events (Trudgill et al., 1983; Beven and Germann, 1982; Smart and Friederich, 1986). Macropore flow is represented by a hydrograph in which the instantaneous outflow rate, Q_{mcrp}, is related to the volume of water in the hydrograph reservoir, V_{mcrp},
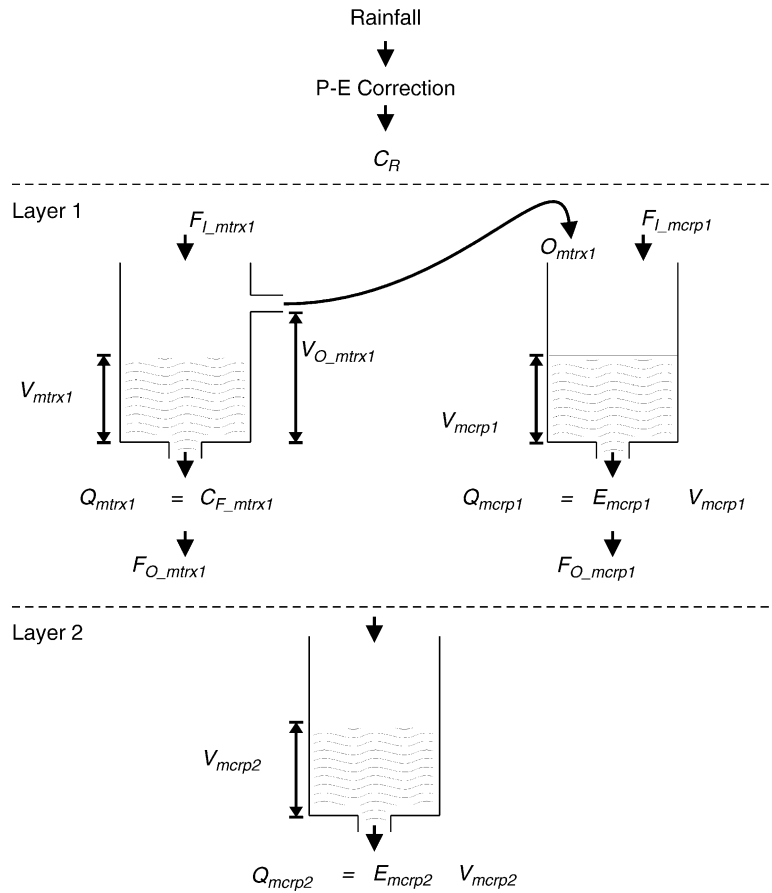
Fig. 5. Diagrammatic representation of the model. Parameters are explained in Table 2 and its design and working are covered in the text.

through a fractional coefficient

$$Q_{\mathrm{mcrp}} = E_{\mathrm{mcrp}} V_{\mathrm{mcrp}} \tag{1}$$

where E_{mcrp} represents the fraction of the volume of water present in the hydrograph leaving the hydrograph per unit time. Given that Q_{mcrp} is the change in volume with time, and V_{mcrp} is also a function of time, Eq. (1) can be written in a differential form as

$$\frac{\mathrm{d}V_{\mathrm{mcrp}}}{\mathrm{d}t} = E_{\mathrm{mcrp}} V_{\mathrm{mcrp}}(t) \tag{2}$$

or, if differentiated again,

$$\frac{\mathrm{d}^2 V_{\mathrm{mcrp}}}{\mathrm{d}t^2} = E_{\mathrm{mcrp}} \frac{\mathrm{d}V_{\mathrm{mcrp}}}{\mathrm{d}t} \tag{3}$$

It proved convenient to solve Eq. (2) numerically. Solutions to Eq. (3), the variation of discharge of time, are shown graphically.

Matrix flow is represented by a hydrograph in which outflow rate is constant, and remains at a constant value as long as there is water in the hydrograph reservoir. Flow rate, Q_{mtrx}, is represented by a simple constant relationship,

$$Q_{\mathrm{mtrx}} = C_{\mathrm{F\_mtrx}} \tag{4}$$

where $C_{\mathrm{F\_mtrx}}$ is the volume of water leaving the hydrograph per unit time.

Each of these two hydrographs represents a reservoir containing waters with fixed Ca composition, equilibrated with soil PCO_2 in layer 1, and a characteristic Mg/Ca and Sr/Ca composition.

The justification for a fixed Ca composition is that there is no seasonal variation in Ca or PCO_2 independent of discharge; this is found to be the pattern at a number of other cave sites, where it can be shown that there is a seasonally buffered CO_2 reservoir (Atkinson, 1977; Fairchild et al., 2000; Spötl et al., 2005). The Ca value is taken as 3 mmol/L, which is close to the highest values encountered for dripwaters at sites B and F3.

It is implicit that the cationic composition characteristic of the macropore reservoir is attained rapidly, because its composition arises from congruent calcite dissolution (on the walls of fissures and other macropores). Since the geometry of these walls only changes slowly, an assumption of a fixed Mg/Ca and Sr/Ca for the macropore reservoir feeding a given drip is reasonable. Water recharging the matrix hydrograph is likely to have already developed such characteristics, either in the soil, or through passing through a fissure, but will tend to develop a characteristically higher content of Mg (and slightly higher Ca) by dissolution of dolomite and/or Sr by dissolution of aragonite. Dolomite dissolution is inevitably slow (Chou et al., 1989) and aragonite will only be preserved in clay layers, low permeability by definition. Hence, there is an association of low permeability parts of the aquifer with higher trace element contents (Baker et al., 2000). The fixed nature of the Mg/Ca and Sr/Ca composition of the matrix reservoir for a given drip is justified in the case of constant flow path and discharge, as used in the model. The notions of fixed end-member reservoirs, mixing conservatively, is to be tested by the modelling.

The model is based on a two-layer representation of the subsurface in which rainfall-derived input passes through hydrographs to supply a single drip site (Fig. 5). The model parameters are represented in Fig. 5, and listed with descriptions in Table 2. The atmospheric precipitation (P) corrected by the calculated evapotranspiration (E) is referred to here as $P-E$. $P-E$ is an imperfect representation of infiltration because of local variation in site characteristics and the variable intensity of rainfall. We therefore tuned the model by introducing a threshold value for $P-E$ before infiltration; this parameter is returned to in the discussion.

Water entering the part of the subsurface of interest at each time step, that is the part of the subsurface represented by the model, is calculated from $P-E$ by a conversion constant, the rainfall coefficient, C_R. The necessity for this constant arises because the catchment area for a given drip cannot be defined geometrically and so an additional mass balance constraint is not available. The model, therefore tunes the output to the mean observed drip discharge, and it is therefore, the variation in discharge, not the mean value, which provides the heuristic value of the model.

The input volume is then split between the two hydrographs in Layer 1 according to the input fraction constants F_{I_mtrx1} and F_{I_mcrp1}. Overflow from the matrix occurs if the volume of water in the matrix flow hydrograph V_{mtrx1}, exceeds the porosity, that is the specified overflow volume, V_{O_mtrx1}. As explained above, water will recharge the matrix via soil macropores and karstic fissures, but the model does not distinguish them as it is assumed that the reservoir characteristics will be attained by the output water from the matrix in either case. Hence, the Layer 1 macropore hydrograph does not include water that recharges matrix, since by definition (Fig. 5) all water from it outflows to Layer 2. Water that has passed through the Layer 1 matrix flow hydrograph exits into Layer 2.

Layer 2 contains one macropore flow hydrograph, the input to which is controlled by the output from each hydrograph in Layer 1, and the output fraction coefficients F_{O_mtrx1} and F_{O_mcrp1}, which allow for a portion of the water leaving each Layer 1 hydrograph to be lost from the system. Much more water would be expected to leave the macropore hydrograph than the seepage hydrograph as a given macropore system probably feeds a number of drips. Outflow from the Layer 2 hydrograph represents a volume of water per time step, which can be converted to a drip rate (measured in drips per second).

The only chemical process that is allowed to occur within this reservoir is precipitation of some $CaCO_3$. The amount of precipitation depends on the reservoir characteristics—the more empty the reservoir, the more $CaCO_3$ precipitation will occur because there will be more air space. This justified by the observed relationship between Ca and discharge (Fig. 3) for sites B and F5 which is used to derive simple

Table 2
Hydrological parameters of the model (see also Fig. 5 and text)

Parameter	Description	Maximum value[a]	Comments	Site B (daily)	Site B	Site F5	Site F3
Surface							
Rainfall	Local measured precipitation data	n/a					
$P-E$	Corrected rainfall		Precipitation minus evaporation calculated by Thornthwaite method				
$P-E$ correction	Threshold		A threshold value to adjust the calculated $P-E$ by a constant value to tune the model	3	19	19	19
C_R	Rainfall coefficient	∞	A coefficient to convert adjusted $P-E$ (mm/week) to a volume of water entering the system of interest (litres). Assumes that the volume of water entering the system of interest varies linearly with $P-E$-corrected rainfall	30.6	21.3	5.06	4.91
Layer 1							
F_{I_mtrx1}	Input fraction	1.0	Fraction of water entering the system from the surface that flows directly into the matrix-flow hydrograph. $F_{I\_mtrx1}+F_{I\_mcrp1}\equiv 1.0$	0.992	0.954	0.6	0.95
V_{mtrx1}	Volume	∞*	Volume of water in matrix-flow hydrograph				
V_{I_mtrx1}	Initial volume	V_{O_mtrx1}	Initial volume of water in matrix-flow hydrograph (value at time zero)	204	118.8	100	5
V_{O_mtrx1}	Overflow volume	∞	Volume at which matrix-flow hydrograph overflows to macropore-flow hydrograph ($=$pore volume in matrix-flow reservoir)	204	142.5	100	5
	Mg/Ca		Mg/Ca in matrix reservoir (Ca$=$3 mmol/L)	0.23	0.23	0.1	0.07
	Sr/Ca		Sr/Ca in matrix reservoir (Ca$=$3 mmol/L)	0.003	0.003	0.002	0.0035
C_{F_mtrx1}	Flow constant	∞	Constant flow rate out of matrix-flow hydrograph	0.06	0.18	0.06	0.2
Q_{mtrx1}	Outflow	C_{F_mtrx1}*	Flow rate out of matrix-flow hydrograph (litres/time step)				
F_{O_mtrx1}	Output fraction	1.0	Fraction of outflow from matrix-flow hydrograph that enters the system in layer 2. Allows a proportion of the output from matrix-flow hydrograph to be lost from the system.	1	1	0.73	1
F_{I_mcrp1}	Input fraction	1.0	Fraction of water entering the system from the surface that flows directly into the matrix-flow hydrograph. $F_{I\_mtrx1}+F_{I\_mcrp1}\equiv 1.0$	0.008	0.045	0.4	0.05
O_{mtrx1}	Overflow input	∞*	Input to macropore-flow hydrograph from overflow of matrix-flow hydrograph				
V_{mcrp1}	Volume	∞*	Volume of water in macropore-flow hydrograph				
V_{I_mcrp1}	Initial volume	∞	Initial volume of water in macropore-flow hydrograph (value at time zero)	6.15	2.97	2.13	2.98
	Mg/Ca		Mg/Ca in macropore reservoir	0.09	0.09	0.05	0.07
	Sr/Ca		Sr/Ca in macropore reservoir	0.0025	0.0025	0.0002	0.0005
E_{mcrp1}	Flow coefficient	1.0	Fraction of V_{mcrp1} that flows out of the hydrograph at each time step	0.24	0.73	0.2	0.37
Q_{mcrp1}	Outflow	∞*	Flow rate out of macropore-flow hydrograph (litres/time step)				
F_{O_mcrp1}	Output fraction	1.0	Fraction of outflow from macropore-flow hydrograph that enters the system in layer 2. Allows a proportion of the output from macropore-flow hydrograph to be lost from the system.	0.102	0.07	0.1	0.0016

(continued on next page)

Table 2 (continued)

Parameter	Description	Maximum value[a]	Comments	Site B (daily)	Site B	Site F5	Site F3
Layer 2							
V_{mcrp2}	Volume	∞ *	Volume of water in macropore-flow hydrograph				
V_{I_mcrp2}	Initial volume	∞	Initial volume of water in macropore-flow hydrograph (value at time zero)	61.6	29.72	0.43	0.4
E_{mcrp2}	Flow coefficient	1.0	Fraction of V_{mcrp2} that flows out of the hydrograph at each time step	0.136	0.41	0.7	0.369
Q_{mcrp2}	Outflow	∞ *	Flow rate out of macropore-flow hydrograph (litres/time step)				

Values marked * are calculated automatically by the model, all others are set by the user.

[a] All minimum values are zero.

algorithms to control the amount of calcite precipitation.

The model is evaluated using an iterative time-series integration of hydrograph responses. Because the sampling interval is longer than a week, most of the modelling has been driven by weekly rainfall data, although some additional work was done on daily data. The model outputs are time-series drip rate and chemical concentration data. In such discrete solution schemes, accuracy is improved by minimising the discrete time-step at which successive calculations are made, however, the models are constrained by the frequency of the input data. It is therefore expected that predicted variations in drip rate will decrease in reliability as the frequency of variation approaches the frequency of the calculation time step.

The fit of the models to the observed drip data was initially optimised manually by user adjustment of the key model parameters. This method, although laborious, provided a good initial fit to the observed data. Subsequently, model parameters were optimised computationally using a random walk method to minimise the difference between model predictions and drip rate observations. Taking the user-derived models as initial guesses, this automatic optimisation
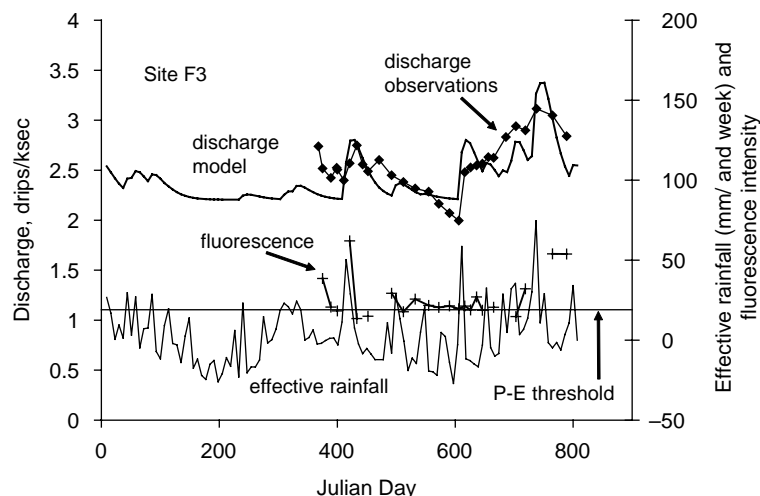

Fig. 6. Time variation of discharge and intensity of fluorescence of dripwaters at site F3 in relation to calculated precipitation minus evaporation (P-E) and modelled discharge. The P-E threshold (19 mm) is derived from the modelling: only values of P-E greater than this lead to short-term increases in observed discharge. Julian Day refers to days since 1.1.1996 in this and later figures. See text for discussion.

method allowed the rapid improvement of model parameters. In the case of site F5, the best-fit model produced by this optimisation was rejected, and another slightly different model accepted in preference due to a better fit to the extremes of the data. This model was chosen by inspection rather than any strict quantitative measure of fit or suitability. However, in future, more complex models, selection criteria may be designed to achieve the same results either through a measure of the statistical properties of the data, or the integration of a fuzzy logic methodology.

6. Model results and discussion

6.1. Site F3

This site shows the lowest drip rate and variation in drip rate of all the studied sites. Fig. 6 illustrates that the drip rate only varied by 50% during the whole monitoring period, indicating a dominance of seepage flow. Nevertheless, the increases in fluorescence intensity seen at periods of higher discharge demonstrate the importance of input of new water from the soil zone (modelled here as the macropore reservoir), rather than pure

piston flow effects. The hydrological model solution shown in Table 2 successfully reproduces the main features of the discharge variation including approximating the dynamic range and the prompt increases in discharge following major infiltration events. However, equally good fit is provided by other model solutions, which involve a long-term drop in storage compared with that at the beginning of 1996 (when there is no observational data). As with the other sites, satisfactory results can only be obtained by introducing a $P-E$ correction (of around 19 mm); otherwise, the influence of more minor rainfall events is too strong. It will be shown later that this feature may merely be an artefact of the use of weekly rather than daily rainfall data.

Fig. 7(a) demonstrates the limited range of variation in Sr content of waters produced by the model compared with that observed. There are two reasons for this. Firstly, there is a temporal change in behaviour: Sr values are constantly low and independent of discharge before day 550, but then become higher and much more responsive to discharge thereafter. Since there is little recharge between days 500 and 600, this can be understood in terms of a threshold to the drainage of a high Sr (at least 0.01 mmol/L) seepage reservoir at low flows. Secondly, it is
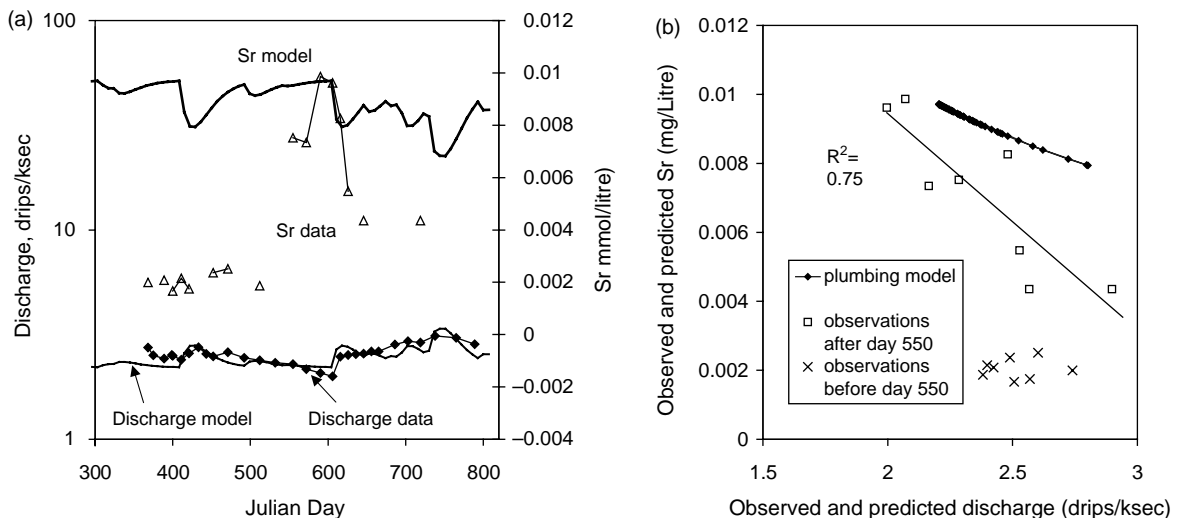

Fig. 7. Observed and modelled discharge, and observed and modelled Sr plotted (a) against time (b) against each other, at site F3. See text for discussion.
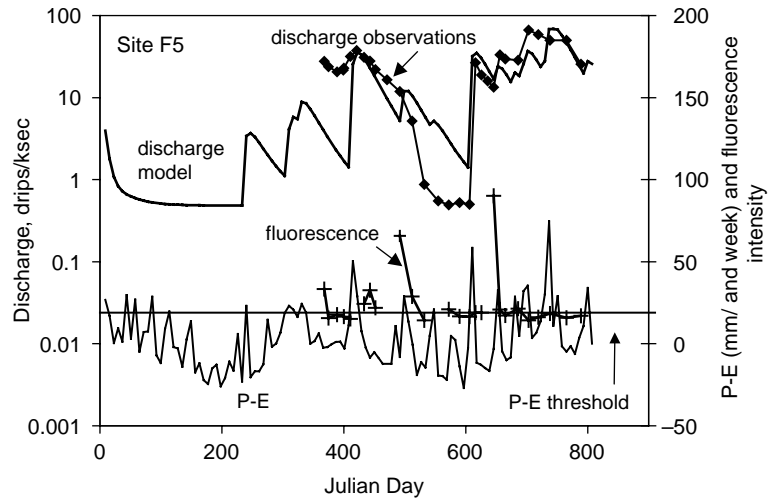
Fig. 8. Equivalent diagram to Fig. 6 for site F5.

impossible to produce a sufficient dynamic range of Sr, essentially because in order to provide a satisfactory model for the discharge, a large component of seepage flow is required throughout. The existence of more than one seepage reservoir suggests an explanation for this feature–that the dynamic range reflects interplay between the two seepage reservoirs. Sr values peak just before the flow minimum and then fall, coincident with the fall in modelled Sr to values intermediate between the composition of the two seepage reservoirs. Once drainage was activated from the highest-Sr

reservoir, it was maintained. This is an important non-linearity in the system.

6.2. Site F5

This site with intermediate behaviour shows a discharge variation of two orders of magnitude, which is matched by the model, as are the timings of change (Fig. 8). The discharge from the seepage reservoir was chosen to match the minimum discharge observed around day 600, but the real system falls to this level
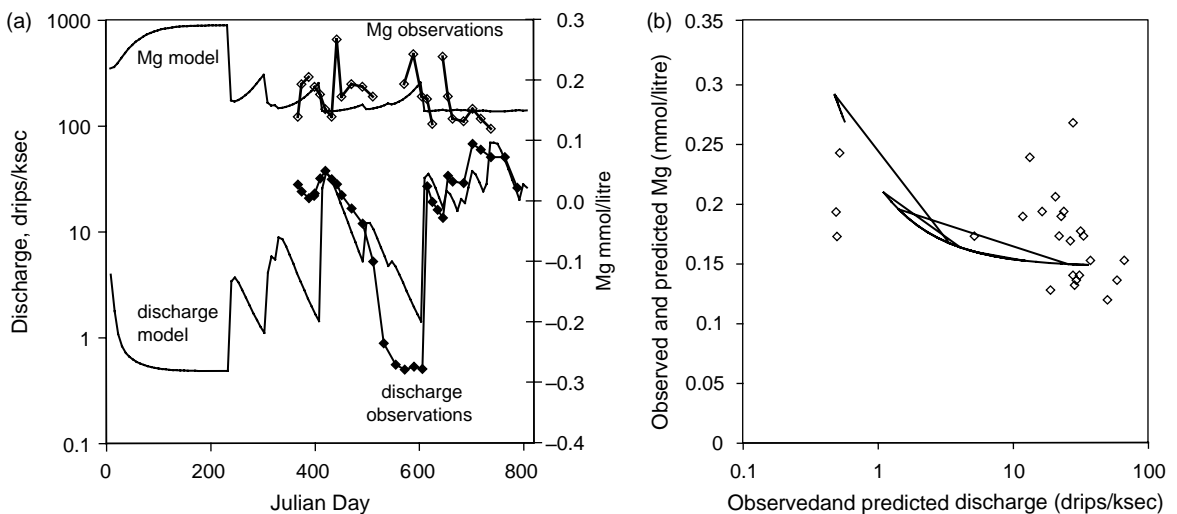

Fig. 9. Equivalent diagram to Fig. 7 for site F5, except that Mg is the plotted hydrochemical variable, rather than Sr.
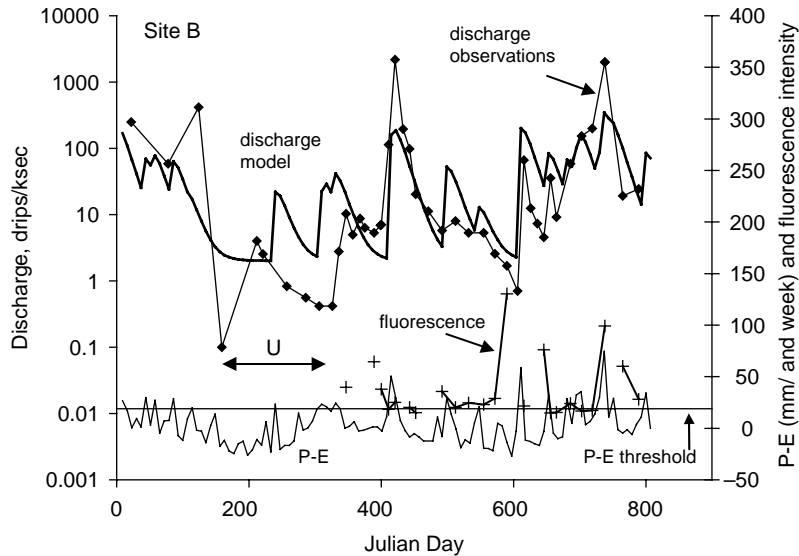
Fig. 10. Equivalent diagram to Fig. 6 for site B.

faster than predicted by the model. The rapid decline in fluorescence also indicates that a rapidly declining discharge component from the soil zone is present. Adjustment of parameters in the present model could not reproduce this feature, which would require an additional hydrograph.

A difference in Mg/Ca ratio between macropore and seepage reservoirs is implied by an inverse relationship between Mg and discharge, apart from an outlying point (Fig. 3(b)). Hence, it is possible to set up the model to show the correct range of Mg (Fig. 9(a)), and Mg does fall appropriately at the two major increases in discharge. However, Mg also rises at some points at high discharge. Although the model results do show some hysteresis effects which broaden the distribution of points (Fig. 9(b)), the presence of some high-Mg points at high discharge clearly points to an additional source, as deduced above. The inverse relationships between Ca and Mg/Ca and Sr/Ca (Fig. 4) imply that this third source has low Ca. Clearly any speleothem deposited from a drip behaving like F5 would not show any clear-cut climatic relationships.

6.3. Site B

This site shows over four orders of magnitude variation in discharge and so the standard 10–20 days observation period is not ideal to capture the variation as is shown by the datalogger data presented below. The hydrological model is able to match the middle range of variation well (Fig. 10), but no combination of parameters allows it to capture the extremes of discharge. Interestingly, there is a general lack of correlation of model and observations within a specific time interval (c. 150–350 days, labelled U on Fig. 10). Near the beginning of this period this site is the driest during the whole interval which suggests a possible explanation: that excess air entered the system causing it to display, in part, underflow behaviour until sufficient recharge had occurred to force it to resume its former behaviour.

Since the failure to capture peak discharge might relate to the averaging effects of using weekly rainfall, calculations were made using daily data. It was found that this slightly increased the dynamic range of discharge to just over two orders of magnitude. The corresponding $P-E$ daily threshold was 3 mm. The reduction in the $P-E$ threshold to a low value is an encouraging result since daily rainfall data reproduces much more closely the individual rainfall events. Fig. 11 shows a comparison of datalogger discharge, daily $P-E$, and data modelled using the daily $P-E$ inputs. It is again found that the middle ranges of discharge are well reproduced by the model. However the logger data
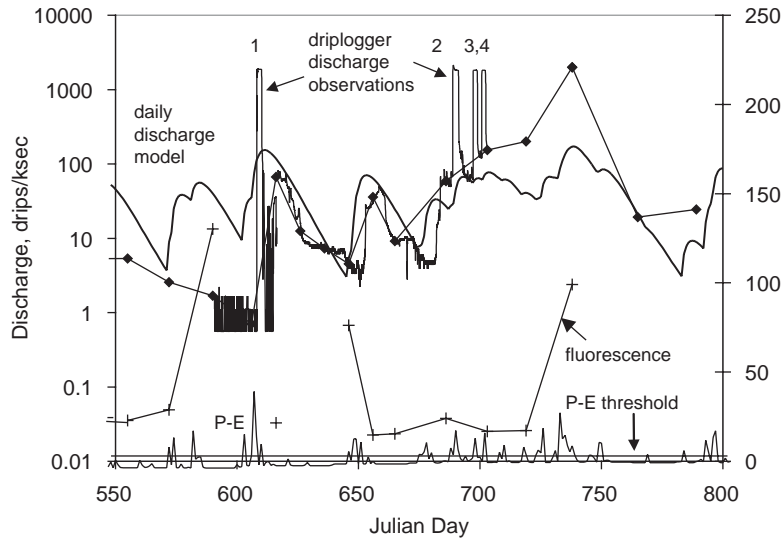
Fig. 11. The same parameters as in Fig. 10, plotted over a restricted time interval and based on daily measurements of precipitation and including quasi-continuously logged discharge. Note that the P-E threshold is now only 3 mm and that rainfall events significantly exceeding this value lead to overflow-type behaviour whereby a conduit delivers a constant high discharge for a short period of time. The discharge model does not include this behaviour, but accounts reasonably well for discharges outside these short periods.

displays several short-lived high-discharge events, which reach a constant discharge ceiling (1–4 on Fig. 11). It is evident that the peak discharge is represented by such short-lived events, which would clearly require an additional hydrograph to be captured by the model. Since the constant high

discharge level implies conduit flow, such a hydrograph would have to have a different parameterization from those used in the model. High fluorescence values, however, are not restricted to the duration of the peak flow events which is consistent with the progressive decline of macropore
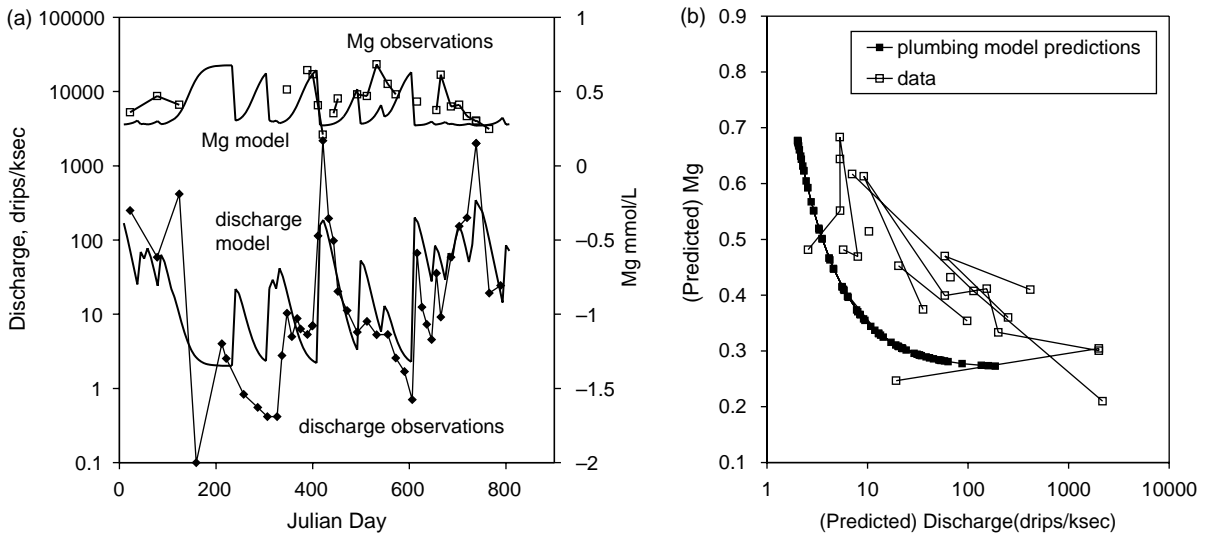

Fig. 12. Equivalent diagram to Fig. 9 for site B.

inputs from the soil zone (e.g. that of day 590 which still records significant soil-derived input from the recharge event on day 582).

Fig. 12 compares the predictions of the model for Mg behaviour with the observations. Although there are some points of good agreement, the data are consistently higher in Mg for a given discharge than would be predicted by the passive conservative mixing in the model set-up. The enhancement in Mg, which is a species more concentrated in the seepage reservoir implies coupling of macropore and seepage reservoirs so as to promote active entrainment of fluids from the latter. Price et al. (2000) described a mechanism (in Chalk) which could be responsible for this behaviour. Fissure flow can commence by gradual wetting up of irregular walls by flow from the matrix, with its characteristic Mg/Ca ratio.

6.4. Discussion

The above evidence demonstrates specific applications and limitations of a two-component linear systems model to the hydrology and hydrogeochemistry of karstic dripwaters at the site. Satisfactory hydrological solutions could be obtained for drips F3 and F5 given certain non-linearities built-in to the model (e.g. a $P-E$ threshold for recharge; overflow design to the hydrographs in layer 1). However, hydrological data from site B and hydrological data from sites F3 and F5 require a third component. Although the optimization methods used during the modelling were unsophisticated, the simple model structure allowed us to establish a limited range of optimal model structures. For a more complex model based on unit hydrographs, a more systematic approach could be offered by the use of genetic algorithms. They allow the application of the same methodology to more complex systems.

Two additional phenomena were recognized which emphasize non-linear aspects of the system. Just such a disruption to the hydrochemical regime can occur by high-flow in subglacial environments (Fairchild et al., 1999), so exceptionally low flows at Browns Folly Mine are associated with thresholds to different behaviour. Thus at site B, discharge did not reflect recharge for a significant period following low-flow, and at site F3 exceptionally low flows allowed the

tapping of a new, very Sr-rich reservoir, from which solutes continued to be entrained following increased discharge. A possible mechanism is the introduction to air to previously saturated parts of the system. The second non-linearity is clear evidence for active entrainment of seepage waters during fissure flow at site B.

The interpretation of surface water hydrology relies heavily on conservative and passive mixing models (Heal et al., 2002; Soulsby et al., 2003), although in the glacial hydrochemistry field, there has been criticism of two-component models (Sharp et al., 1995), not least because of the great variability in source waters in geometrically and materially complex near-surface environments. Brown et al. (1996) focused on the occurrence of post-mixing chemical reactions as a barrier to interpretation of sources, but in our case, calcite precipitation has been recognized and explicitly allowed for in the model. The more fundamental problem for the linear systems approach is that of fluid interchange between fissures and matrix.

The original question posed by this research relates to the significance of variations with time in elemental ratios such as Sr/Ca and Mg/Ca which would lead to corresponding temporal changes in the calcium carbonate of stalagmites and stalactites. These ratios were inferred to be higher at low discharge conditions by Fairchild et al. (2000) for three reasons: (1) selective leaching from soils, (2) enhanced dissolution of phases, such as dolomite, with slower dissolution kinetics, and (3) calcite precipitation along the flowpath. The study of Baker et al. (2000) in Mesozoic bedrock emphasizes also the preferential derivation of high trace element to Ca ratios by weathering of metastable carbonate in low permeability matrix. The study of Brown's Folly waters show that many of the drips, particularly those with strongly varying discharge, display positive covariation of Ca which can be interpreted as related to factor (3). There is also enhancement in Mg/Ca or Sr/Ca, or both due to source effects, with higher contributions from seepage reservoirs at low flow. The above discussion shows that the variations in Mg/Ca and Sr/Ca chemistry can be understood by a combination of: (a) linear systems response to periods of recharge (the fit of the hydrological model), (b) interaction between reservoirs (e.g. Mg data of Fig. 12(b)), and (c) temporal

discontinuities in source or flow rate following periods of exceptionally low discharge (e.g. Sr data of Fig. 7). For drips B and F3, variations in trace element ratios track dry periods and the onset of particularly high ratios is a particularly robust marker of low-flow conditions. The behaviour of F5 is more complex and no clear climatic responses are apparent. Even in the better cases, however, a linear relationship to rainfall regime is not displayed and some complexities should be expected. This may be resolvable in the case of stalagmites by monitoring of the feeding drip, or by extracting different causes of variation by multi-parameter studies.

In this study, the combination of information on discharge, elemental geochemistry, and fluorescence has proved powerful in evaluating the extent to which a linear systems model is appropriate for karstic dripwaters. The data-model comparison clearly illustrates the overall pattern of quasi-linear behaviour, which is reassuring for palaeohydrological reconstruction. However, there are also a number of important non-linear features apparent in both hydrology and, especially, in hydrochemistry. Non-linearities in karst hydrology have been recognised elsewhere in high temporal resolution discharge series of both karstic springs and cave drips (Labat et al., 2000a,b, 2002; Baker and Brunsdon, 2003). These non-linearities provide valuable pointers to processes that would need to be built into future more sophisticated *distributed* models (Beven, 2002) of this aquifer. High-resolution and automated sampling would clearly help significantly in developing a more detailed understanding of the operation of karstic systems.

Acknowledgements

References

Annable, W.K., Sudicky, E.A., 1999. On predicting contaminant transport in carbonate terrains: Behavior and prediction. In: Palmer, A.N., Palmer, M.V., Sasowsky, D. (Eds.), Karst Modeling. Karst Waters Institute Special Publication 5, Charles Town, West Virginia, pp. 133–145.

Atkinson, T.C., 1977. Carbon dioxide in the atmosphere of the unsaturated zone: An important control of groundwater hardness in limestones. Journal of Hydrology 35, 111–123.

Baker, A., Genty, D., 1999. Fluorescence wavelength and intensity variations of cave waters. Journal of Hydrology 217, 19–34.

Baker, A., Brunsdon, C., 2003. Non-linearities in drip water hydrology: An example from Stump Cross Caverns Yorkshire. Journal of Hydrology 277, 151–163.

Baker, A., Barnes, W.L., Smart, P.L., 1997. Stalagmite Drip Discharge and Organic Matter Fluxes in Lower Cave Bristol. Hydrological Processes 11, 1541–1555.

Baker, A., Mockler, N.J., Barnes, W.L., 1999. Fluorescence intensity variations of speleothem-forming groundwaters: Implications for paleoclimate reconstruction. Water Resources Research 35, 407–413.

Baker, A., Genty, D., Fairchild, I.J., 2000. Hydrological characterisation of stalagmite drip waters at Grotte de Villars, Dordogne, by the analysis of inorganic species and luminescent organic matter. Hydrology and Earth System Sciences 4, 439–449.

Beven, K.J., 2001. Rainfall-Runoff Modelling. Wiley, New York.

Beven, K.J., 2002. Towards an alternative model for a physically based digitally simulated hydrological response modelling system. Hydrological Processes 16, 189–206.

Beven, K., Germann, P., 1982. Macropores and water flow in soils. Water Resources Research 18, 1311–1325.

Bottrell, S.H., Atkinson, T.C., 1992. Tracer study of flow and storage in the unsaturated zone of a karstic limestone aquifer. In: Hötzl, H., Werner, A. (Eds.), Tracer Hydrology. Balkema, Rotterdam, pp. 207–211.

Brown, G.H., Tranter, M., Sharp, M.J., 1996. Experimental investigations of the weathering of suspended sediment by Alpine glacial meltwater. Hydrological Processes 10, 579–597.

Buttell, J.M., 1994. Isotope hydrograph separations and rapid delivery of pre-event water from drainage basins. Progress in Physical Geography 18, 16–41.

Chanat, J.G., Rice, K.C., Hornberger, G.M., 2002. Consistency of patterns in concentration-discharge plots. Water Resources Research 38, 8. doi:10.1029/2001WR000971.

Chou, L., Garrels, R.M., Wollast, R., 1989. Comparative study of the kinetics and mechanisms of dissolution of carbonate minerals. Chemical Geology 78, 269–282.

Fairchild, I.J., Killawee, J.A., Sharp, M.J., Spiro, B., Hubbard, B.P., Lorrain, R.D., Tison, J.-L., 1999. Solute generation and transfer from a chemically reactive Alpine glacial-proglacial system. Earth Surface Processes and Landforms 24, 1189–1211.

Fairchild, I.J., Borsato, A., Tooth, A.F., Frisia, S., Hawkesworth, C.J., Huang, Y., McDermott, F., Spiro, B., 2000. Controls on trace element (Sr-Mg) compositions of carbonate cave waters: Implications for speleothem climatic records. Chemical Geology 166, 255–269.

Fairchild, I.J., Baker, A., Borsato, A., Frisia, S., Hinton, R.W., McDermott, F., Tooth, A.F., 2001. High-resolution, multiple-trace-element variation in speleothems. Journal of the Geological Society, London 158, 831–841.

Genty, D., Deflandre, G., 1998. Drip flow variations under a stalactite of the Père Noël cave (Belgium). Evidence of seasonal variations and air pressure constraints. Journal of Hydrology 211, 208–232.

Green, G.W., Donovan, D.T., 1969. The Great Oolite of the Bath area. Bulletin of the Geological Survey of Great Britain 30, 1–63.

Heal, K.V., Kneale, P.E., McDonald, A.T., 2002. Manganese in runoff from upland catchments: Temporal patterns and controls on mobilization. Hydrological Sciences Journal 47, 769–780.

Huang, Y., Fairchild, I.J., 2001. Partitioning of Sr^{2+} and Mg^{2+} into calcite under karst-analogue experimental conditions. Geochimica Cosmochimica Acta 65, 47–62.

Huang, Y., Fairchild, I.J., Borsato, A., Frisia, S., Cassidy, N.J., McDermott, F., Hawkesworth, C.J., 2001. Seasonal variations in Sr, Mg and P in modern speleothems (Grotta di Ernesto, Italy). Chemical Geology 175, 429–448.

Labat, D., Ababou, R., Mangin, A., 2000a. Rainfall-runoff relations for karstic springs. Part I: Convolution and spectral analysis. Journal of Hydrology 238, 123–148.

Labat, D., Ababou, R., Mangin, A., 2000b. Rainfall-runoff relations for karstic springs. Part II: continuous wavelet and discrete orthogonal multi-resolution analyses. Journal of Hydrology 238, 149–178.

Labat, D., Mangin, A., Ababou, R., 2002. Rainfall-runoff relations for karstic springs: Multifractal analysis. Journal of Hydrology 256, 176–195.

Long, A.J., Derickson, R.G., 1999. Linear systems analysis in a karst aquifer. Journal of Hydrology 219, 206–217.

Long, A.J., Putnam, L.D., 2004. Linear model describing three components of flow in karst aquifers using ^{18}O data. Journal of Hydrology 296, 254–270.

Maloszewski, P., Stichler, W., Zuber, A., Rank, D., 2002. Identifying the flow systems in a karstic-fissured-porous aquifer, the Schneealpe, Austria, by modelling of environmental ^{18}O and ^{3}H isotopes. Journal of Hydrology 256, 48–59.

McMillan, E., Fairchild, I. J., Frisia, S., Borsato, A., 2005. Calcite-aragonite trace element behaviour in annually layered speleothems: Evidence of drought in the Western Mediterranean 1200 years ago, Journal of Quaternary Science.

Morse, J.W., Bender, M.L., 1990. Partition coefficients in calcite: Examination of factors influencing the validity of experimental results and their application to natural systems. Chemical Geology 82, 265–277.

Perrin, J., Jeannin, P.-V., Zwahlen, F., 2003. Epikarst storage in a karst aquifer: A conceptual model based on isotopic data, Milandre test site, Switzerland. Journal of Hydrology 279, 106–124.

Price, M., Low, R.G., McCann, C., 2000. Mechanisms of water storage and flow in the unsaturated zone of the Chalk aquifer. Journal of Hydrology 233, 54–71.

Self, C.A., 1995. The relationship between the gull cave Sally's Rift and the development of the River Avon east of Bath. Proceedings of the University of Bristol Spelaeological Society 20, 91–108.

Selroos, J.-O., Walker, D.D., Ström, A., Gylling, B., Follin, S., 2002. Comparison of alternative modelling approaches for groundwater flow in fractured rock. Journal of Hydrology 257, 174–188.

Sharp, M., Brown, G.H., Tranter, M., Willis, I.C., Hubbard, B., 1995. Comments on the use of chemically based mixing models in glacier hydrology. Journal of Glaciology 41, 241–246.

Shaw, E.M., 1994. Hydrology in Practice. Chapman and Hall.

Smart, P.L., 1977. Catchment delimination in karst areas by the use of quantitative tracer methods, Proceedings 3rd International Syposium of Underground Water Tracing. Ljubljaana-Bled, Slovenia pp. 291–298..

Smart, C.C., 1999. Subsidiary conduit systems. In: Palmer, A.N., Palmer, M.V., Sasowsky, D. (Eds.), Karst Modeling. Karst Waters Institute Special Publication 5, Charles Town, West Virginia, pp. 146–157.

Smart, P.L., Friederich, H., 1986. Water movement and storage in the unsaturated zone of a maturely karstified aquifer, Mendip Hills, England, Proceedings of the Conference on Environmental Problems in Karst Terrains and their Solutions. National Water Wells Association, Bowling Green, Kentucky pp. 57–87.

Soulsby, C., Rodgers, P., Smart, R., Dawson, J., Dunn, S., 2003. A tracer-based assessment of hydrological pathways at different spatial scales in a mesoscale Scottish catchment. Hydrological Processes 17, 759–777.

Spötl, C., Fairchild, I. J. Tooth, A. F., 2005. Speleothem deposition in a dynamically ventilated cave, Obir Caves (Austrian Alps). Evidence from cave air and drip water monitoring. Geochimica et Cosmochimica Acta.

Tooth, A.F., Fairchild, I.J., 2003. Soil and karst aquifer hydrological controls on the geochemical evolution of speleothem-forming drip waters, Crag Cave, southwest Ireland. Journal of Hydrology 273, 51–68.

Trudgill, S.T., Pickles, A.M., Smettern, K.R.J., Crabtree, R.W., 1983. Soil-water residence time and solute uptake. 1. Dye tracing and rainfall events. Journal of Hydrology 60, 279–285.

Vaute, L., Drogue, C., Garrelly, L., Ghelfenstein, M., 1997. Relations between the structure of storage and the transport of chemical compounds in karstic aquifers. Journal of Hydrology 199, 221–236.

Yue, S., Hashino, M., 2000. Unit hydrographs to model quick and slow runoff components of streamflow. Journal of Hydrology 227, 195–206.